Available online at www.sciencedirect.com

SciVerse ScienceDirect

Energy Procedia 10 (2011) 232 – 237

Energy Procedia

European Materials Research Society Conference
Symp. Advanced Inorganic Materials and Concepts for Photovoltaics

High-resolution laser beam induced current measurements on $Cd_{0.9}Zn_{0.1}S$/ CdTe solar cells

W. S .M. Brooks*, S. J. C. Irvine, V. Barrioz

Centre for Solar Energy Research, OpTIC Glyndwr, St Asaph Business Park, St Asaph, Denbighshire, LL17 0JD, UK

Abstract

An assessment of $Cd_{0.9}Zn_{0.1}S$ window layer thickness and its impact on photoresponse uniformity in CdTe thin film photovoltaic (PV) devices is presented. A triple-wavelength laser beam induced current (LBIC) system provided a spatially resolved photocurrent mapping technique. Three diode lasers; λ = 405, 658, 810nm gave photon absorption and carrier generation characteristics over the spectral range of the $Cd_{0.9}Zn_{0.1}S$/ CdTe devices. Two contrasting device structures were grown by metal-organic chemical vapour deposition (MOCVD), where the uniformity of the $Cd_{0.9}Zn_{0.1}S$ window layer was known to vary: 1. uniform 240 nm $Cd_{0.9}Zn_{0.1}S$/ 2 µm CdTe and 2. a poorly nucleated 40 - 300 nm $Cd_{0.9}Zn_{0.1}S$/ 2 µm CdTe. Calculated photon penetration depths, δ_p allowed for the separation of identified defects within the device cross-section. $Cd_{0.9}Zn_{0.1}S$ pin holes were identified in 240 nm $Cd_{0.9}Zn_{0.1}S$/ 2 µm CdTe where 405 nm photon 'punch-through' into the absorber material was observed. These pin holes also led to a localised reduction in photoresponse at λ = 658 and 810 nm. In the device structure where the $Cd_{0.9}Zn_{0.1}S$ window layer thickness was known to vary from 40 to 300 nm, CdTe pin holes were identified where localised ~ 50 µm regions of reduced photoresponse, at all wavelengths were observed. Local variations in both $Cd_{0.9}Zn_{0.1}S$ and CdTe thickness were also identified where variable absorption led to a distribution of LBIC photoresponse. It was demonstrated that reduced photoresponse uniformity at all incident wavelengths was related to reduced device shunt resistance, R_{sh} and open-circuit voltage, V_{oc}.

Selection and/or peer-review under responsibility of Organizers of European Materials Research Society (EMRS) Conference: Symposium on Advanced Inorganic Materials and Concepts for Photovoltaics.

Keywords: laserbeam induced current, $Cd_{0.9}Zn_{0.1}S$, defects, photoresponse.

* Corresponding author. Tel.: 0044-(0)1745 535 213; fax: 0044-(0)1745 535 101
E-mail address: chp605@bangor.ac.uk.

1876-6102 © 2011 Published by Elsevier Ltd. Selection and/or peer-review under responsibility of Organizers of European Materials Research Society (EMRS) Conference: Symposium on Advanced Inorganic Materials and Concepts for Photovoltaics. Open access under CC BY-NC-ND license.
doi:10.1016/j.egypro.2011.10.183

1. Introduction

CdTe has been at the centre of photovoltaic (PV) materials research for several years. It's near optimum band gap of 1.45 eV and high absorption coefficient makes it a promising material for PV applications. The maximum reported CdTe cell efficiency of 16.5 % [1] has remained unchanged since 2004; this falls significantly short of the theoretical maximum of ~ 30 %. In attempting to understand this discrepancy between the theoretical and the best experimental efficiencies more detailed measurements of the special variations in cell properties are required. Routine PV device characterisation techniques often include light and dark current-voltage (I-V) measurements and external quantum efficiency (EQE) measurements. These provide key parameters describing the performance of a PV cell, but inherently these techniques average measurements over the photoactive region of the cell, often limited by the front or back contact area. To achieve a degree of spatial separation and resolution, so that spatially resolved defects can be detected, requires a different approach. The beam induced current techniques [2, 3] have been demonstrated in several different forms; from electron beam induced current (EBIC), where an electron beam excites minority carrier generation [4], to optical beam induced current (OBIC), where an optical beam is used to achieve the same excitation process [5]. The optical beam in the latter example is typically generated via a monochromated white light source. An advantageous alternative to this is a single-mode fibre-coupled laser beam, where an easily manipulated, highly collimated and narrow band width beam, lends itself well to this application. This approach is known as laser beam induced current (LBIC) [6]. The LBIC technique can generate high resolution, spatially resolved, photoresponse measurements, where carrier generation uniformity can be mapped over an XY range. Further to XY spatial resolution, the LBIC generation depth can be calculated based on the wavelength dependent photon penetration depth, $\delta_{p.}$ This allows for defect detection within a device cross-section. All PV devices used in the investigation were grown in superstrate configuration using metal organic chemical vapour deposition (MOCVD). $Cd_{0.9}Zn_{0.1}S$ is used as the window layer material [7], which has been demonstrated to broaden the optical band gap from 2.4 eV (typical for CdS) to 2.7 eV [8]. The thickness of the $Cd_{0.9}Zn_{0.1}S$ window layer requires a balance of optical and electronic properties, thin enough not to block photons that could be contributing to the cell output and thick enough to ensure good pn junction quality. To investigate the effect of window layer uniformity on device photoresponse uniformity, 0.5 x 0.5 mm^2 LBIC maps on full $Cd_{0.9}Zn_{0.1}S$ and 2 μm CdTe devices were produced, where the $Cd_{0.9}Zn_{0.1}S$ layer thickness was (a) 240 nm and (b) variably nucleated with thickness ranging from 40 - 300 nm.

2. Experimental

The reader is referred to Irvine et al [9] and Barrioz et al [10] for details concerning material structure, composition and thin film deposition. The laser beam induced current setup, used 3 single-mode fibre-coupled diode laser modules, directed into a collimating lens and directional stages followed by an Olympus LUCPlanFl long-working distance dry objective lens. This enabled focussing of the beam to $1/e^2$ beam widths = 10 μm. A sample stage allowed electrical contacting to front and back cell contacts, this stage was mounted onto a manual z-translation stage and automated XY translation stage. Z translation enabled the sample to be moved into and out of the focal point of the incident laser beam, where x and y translation allowed for the sample to be passed beneath the incident laser beam in a pre-defined raster pattern, an XY map of device photoresponse could then be generated. Data acquisition was fully software automated, and XYZ data was plotted using DPlot software. Beam widths were calculated from the marginal distribution of the incident beam between an on and off contact area over a single-axis line scan, this provided a reliable method to extract the $1/e^2$ beam width. Incident power densities were calculated using a calibrated silicon photodetector. Irradiance densities were set to an equivalence of 100 mW cm^{-2}, or 1 sun. All LBIC maps were scanned over a 0.5 x 0.5 mm^2 area at three incident wavelengths; λ = 405, 658 and 810 nm. Light and dark current – voltage (I-V) measurements were recorded at 25 °C

using an Abet Technologies solar simulator, irradiance was calibrated to AM1.5 using a Fraunhofer ISE reference cell. A custom I-V setup and software, using a Keithley 2400 source meter, provided J-V plots from which device performance parameters were derived. Wavelength dependent CdTe absorption coefficients, α, were calculated using Beer- Lambert's law;

$$I = I_o\, e^{-\alpha d} \quad [1]$$

This allowed the derivation of photon penetration depth,

$$\delta_p = 1/\alpha \quad [2]$$

where transmission, I, through a full device structure, was measured using a silicon photodetector and picoammeter. The light incident, I_o on the CdTe absorber layer was determined using a 240 nm $Cd_{0.9}Zn_{0.1}S$ on ITO on glass standard, this accounted for reflection and absorption losses attributable to both the transparent conducting oxide (TCO) layer (ITO) and the $Cd_{0.9}Zn_{0.1}S$ window layer. Each layer thickness, d, was determined from step profile measurements using a Veeco Dektak 150 profilometer.

3. Results and Discussion

3.1 Photon penetration depth

Figure 1 shows the calculated photon penetration depth, δ_p in a device using a 240 nm $Cd_{0.9}Zn_{0.1}S$ window layer, overlaid onto a cross-sectional SEM image of a full $Cd_{0.9}Zn_{0.1}S$ / CdTe device structure [11]. At incident wavelength, λ = 405 nm, 1 – (1/e) photons will have been absorbed at a CdTe cross-sectional depth of 213 nm, indicating that the LBIC measurement at this wavelength will be sensitive to $Cd_{0.9}Zn_{0.1}S$ absorption and very shallow CdTe absorption, with close proximity to the depletion region. At λ = 658 nm and 810 nm, δ_p is measured at 1097 nm and 2005 nm respectively, indicating that LBIC photoresponse measurements at these wavelengths are within the spectral response region of the CdTe absorber layer. At λ = 658 nm the LBIC measurement will be sensitive to bulk CdTe defects and at λ = 810 nm, sensitive to defects towards the back surface of the device.

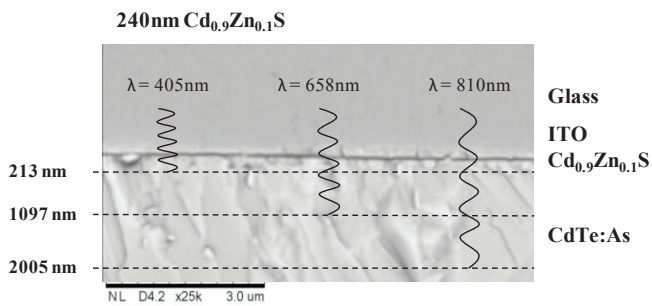

Figure 1. Penetration depths within CdTe device structures using a 240 nm $Cd_{0.9}Zn_{0.1}S$ window layer at incident laser beam wavelengths; 405, 658 and 810 nm.

3.2 Photoresponse uniformity in 240 nm $Cd_{0.9}Zn_{0.1}S$ / 2μm CdTe

Figure 2 shows 0.5 x 0.5 mm LBIC maps from a 240 nm $Cd_{0.9}Zn_{0.1}S$ and 2 μm CdTe device at incident wavelengths, λ = (a) 405 nm, (b) 658 nm and (c) 810 nm. Photoresponse is characterised by two primary observations:

- A majority area of relatively uniform photoresponse at all 3 incident wavelengths.
- The identification of pinhole defects (labelled with arrows).

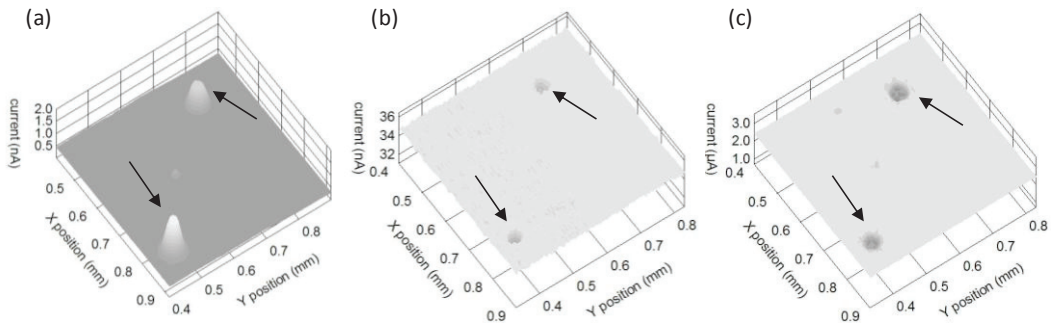

Figure 2. LBIC maps over 0.5 x 0.5 mm area on 240 nm $Cd_{0.9}Zn_{0.1}S$ / 2μm CdTe at (a) 405 nm (b) 658 nm and (c) 810 nm incident laser wavelengths.

The plateau LBIC response at all wavelengths indicates uniform photoresponse at the 3 generation depths described in Fig 1. A low blue response corresponds with high absorption in the $Cd_{0.9}Zn_{0.1}S$ window layer, where conversely, red and IR transmit through the $Cd_{0.9}Zn_{0.1}S$ but are highly absorbing in the CdTe to produce relatively higher LBIC responses. The LBIC identified defects highlighted in Fig 2 show that photoresponse is affected at all incident wavelengths, though the way in which the defect impacts the LBIC response does vary. At λ = 405 nm the defect is observed as a high 'spike' in photoresponse whereas, at λ = 658 nm and 810 nm, at the same XY coordinates the defect is seen as a 'dip' in photoresponse. The triple-wavelength LBIC technique provides a diagnostic route to identifying the origin of the pin-hole defects within the cross-sectional structure of the device. The defects identified in Fig 2 indicate that ~ 50 μm diameter pin holes in the $Cd_{0.9}Zn_{0.1}S$ window are responsible, where reduced $Cd_{0.9}Zn_{0.1}S$ absorption leads to increased LBIC response at these localised areas. These $Cd_{0.9}Zn_{0.1}S$ window layer defects are also shown to affect wavelengths that are absorbing in the CdTe absorber layer (λ = 658 and 810 nm), where a pin hole in the $Cd_{0.9}Zn_{0.1}S$ window layer is shown to reduce photocurrent in the CdTe, indicating that these regions represent localised areas where either carrier generation or minority carrier diffusion is poor.

3.3 Photoresponse uniformity in 40-300 nm $Cd_{0.9}Zn_{0.1}S$ / 2μm CdTe

Figure 3 (a) – (c) show 0.5 x 0.5 mm LBIC maps of a 2 μm CdTe device incorporating a poorly nucleated $Cd_{0.9}Zn_{0.1}S$ window layer where thickness was known to vary from 40 to 300 nm. LBIC responses at all wavelengths contrast from the results shown in section 3.2; where, most notably, the presence of $Cd_{0.9}Zn_{0.1}S$ window layer pin holes were identified. Figure 3 shows pin hole defects at all incident wavelengths, though contrasting from Fig 2 by appearing as drops in LBIC response at 405 nm as well as 658 nm and 810 nm. This indicates that pin holes in the CdTe, causing very low absorption, are leading to a sharp drop in LBIC photoresponse at all wavelengths. Furthermore, the $Cd_{0.9}Zn_{0.1}S$ thickness distribution leads to a variable LBIC response over the full scanned area at all wavelengths; this is in

contrast to the plateau-type response found in Fig 2. Two different regions in Fig 3 are highlighted where thickness variations relating to both the $Cd_{0.9}Zn_{0.1}S$ and CdTe layers can be seen; region 1 shows a pin hole defect where the surrounding LBIC response varies in each map. At λ = 405 nm (Fig 3 (a)) the average LBIC response was low, indicative of increased blue absorption and a thicker $Cd_{0.9}Zn_{0.1}S$ layer. At λ = 658 nm (Fig 3 (b)) an increased LBIC response is measured, in contrast, at λ = 810 nm (Fig 3 (c)) a relatively low LBIC response was measured, this indicates that increased red but reduced IR absorption was occurring. This result can be explained by a localised region (over the scan area) of thin CdTe where 1 - (1/e) absorption at 810 nm requires 2005 nm of CdTe. In contrast, region 2 in Fig 3 shows a relatively high response region surrounding the pin hole defect in each LBIC map, giving a 'volcano' effect. In Fig 3 (a) this is consistent with a thinner $Cd_{0.9}Zn_{0.1}S$ layer, leading to reduced blue absorption. At λ = 658 and 810 nm, a relative increase in local photoresponse can be explained by increased absorption due to a localised region of thicker CdTe which is leading to a higher LBIC response at both wavelengths.

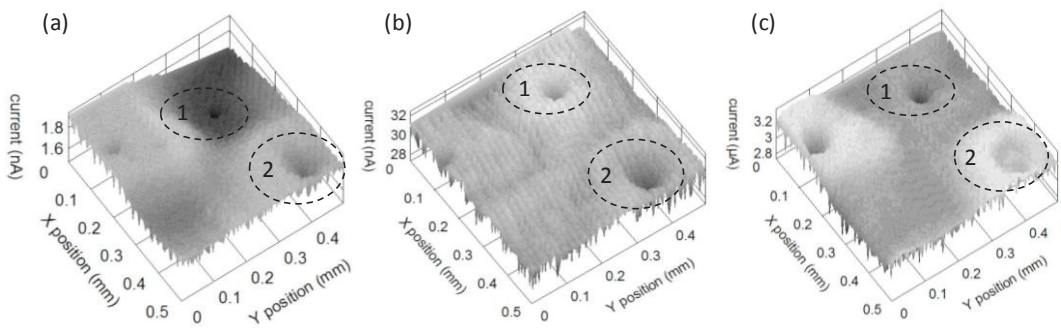

Figure 3. LBIC maps over 0.5 x 0.5 mm area on variably nucleated $Cd_{0.9}Zn_{0.1}S$ / 2μm CdTe at (a) 405 nm (b) 658 nm and (c) 810 nm incident laser wavelengths.

3.4 Light/ dark current voltage (I-V) measurements

Table 1 shows the device parameters derived from current – voltage (I-V) measurements over full 5 x 5 mm^2 contact areas. The device incorporating a variably nucleated $Cd_{0.9}Zn_{0.1}S$ window layer leads to performance losses in both fill factor (FF) and open-circuit voltage (V_{oc}) when compared to the device with a relatively uniform 240 nm $Cd_{0.9}Zn_{0.1}S$ window layer. FF losses in these devices can be largely attributed to low shunt resistance (R_{sh}) which corresponds to the observed variability in window layer and absorber thickness over the scanned areas in addition to the CdTe pin holes.

Table 1. device performance parameters derived from current – voltage (I-V) measurements of devices used for LBIC study.

Device	**η %**	**J_{sc} mA cm^{-2}**	**V_{oc} mV**	**FF %**	**R_s Ω cm^2**	**R_{sh} Ω cm^2**
240 nm $Cd_{0.9}Zn_{0.1}S$ / 2 μm CdTe (Fig 2)	10.9	23.0	667	70.9	2.6	2004
40-300 nm $Cd_{0.9}Zn_{0.1}S$ / 2 μm CdTe (Fig 3)	8.3	23.8	626	56.0	4.0	719

V_{oc} is also demonstrated to decrease in the device with the poorly nucleated $Cd_{0.9}Zn_{0.1}S$ window layer. This is likely related to the reduced R_{sh} where increased recombination, is leading to a reduced minority carrier lifetime. This will in turn increase the reverse saturation current and act to reduce the overall device V_{oc}.

4. Conclusions

A triple wavelength laser beam induced current technique has been used to assess the impact that $Cd_{0.9}Zn_{0.1}S$ window layer uniformity has on (a) photoresponse uniformity and (b) overall device performance. Wavelength dependent penetration depths for each of the lasers were determined, allowing for the evaluation of each LBIC map in terms of physical device parameters, such as layer thickness and photon absorption. It has been shown that a uniform 240 nm $Cd_{0.9}Zn_{0.1}S$ window layer leads to increased photoresponse uniformity at the incident wavelengths, λ = 405, 658 and 810 nm used. Though a majority of the area produced high LBIC response uniformity, pin holes in the $Cd_{0.9}Zn_{0.1}S$ layer were identified using the triple wavelength technique. A variably nucleated $Cd_{0.9}Zn_{0.1}S$ window layer where thickness varied from 40 – 300 nm demonstrated (a) low photoresponse uniformity at all wavelengths and (b) the presence of pin-holes in the CdTe absorber layer. Using the LBIC technique these photoresponse non-uniformities were related to thickness non-uniformities in both $Cd_{0.9}Zn_{0.1}S$ and CdTe layers, where variable absorption and a distribution of LBIC responses at all wavelengths were observed. Poor photoresponse uniformity highlighted by the LBIC measurements were shown to relate to both a reduced FF and V_{oc}. Increased recombination in the device incorporating the variably nucleated $Cd_{0.9}Zn_{0.1}S$, is suggested as a viable cause for the deterioration in open-circuit voltage.

Acknowledgements

The authors would like to thank the Engineering and Physical Sciences Research Council (EPSRC), UK for funding the SUPERGEN PV21 project, making this work possible, and all the members of the CSER group for technical support and guidance.

References

1. Wu, X., *High-efficiency polycrystalline CdTe thin-film solar cells.* Solar Energy, 2004. **77**: p. 803-814.
2. Zook, J.D., *Theory of beam-induced current in semiconductors.* Applied Physics Letters, 1983. **42**: p. 602-604.
3. Marek, J., *Light-beam-induced current characterization of grain boundaries.* Journal of Applied Physics, 1983. **55**: p. 318-326.
4. Edwards, P.R., Galloway, S.A., Durose, K., *EBIC and luminescence mapping of CdTe/CdS solar cells.* Thin Solid Films, 2000. **361-362**: p. 364-370.
5. Major, J.D., Durose, K., *Study of buried junction and uniformity effects in CdTe/CdS solar cells using a combined OBIC and EQE apparatus.* Thin Solid Films, 2008. **517**: p. 2419-2422.
6. Hiltner, J.F., *Investigation of Spatial Variations in Collection Efficiency of Solar Cells*. 2001, Colorado State University.
7. Jones, E.W., Barrioz, V., Irvine, S.J.C., Lamb, D., *Towards ultra-thin CdTe solar cells using MOCVD.* Thin film Solids, 2009. **517**(7): p. 2226-2230.
8. Xia, W., Welt, J.A., Lin, H., Wu, H.N., Ho, M.N., Tang, C.W., *Fabrication of $Cd_{1-x}Zn_xS$ films with controllable zinc doping using a vapor zinc chloride treatment.* Solar Energy Materials and Solar Cells 2010. **94**: p. 2113-2118.
9. Irvine, S.J.C., Barrioz, V., Lamb, D., Jones, E.W., Rowlands-Jones, R.L., *MOCVD of thin film photovoltaic solar cells - Next-generation production technology.* Journal of Crystal Growth, 2008. **310**(23): p. 5198 - 5203.
10. Barrioz, V., Proskuryakov, Y.Y., Jones, E.W., Major, J., Irvine, S.J.C., Durose, K., Lamb, D.A., *Highly arsenic doped CdTe layers for the back contacts of CdTe solar cells.* Mat. Res.Soc Symp. Proc, 2007. **1012**: p. Y12-08.
11. Brooks, W.S.M., Irvine, S. J. C., Barrioz, V., *Laser Beam Induced Current Measurements of $Cd_{0.9}Zn_{0.1}S$/ CdTe Solar Cells.* Solar Energy Materials & Solar Cells, 2011. **submitted**